

## RESEARCH OUTPUTS / RÉSULTATS DE RECHERCHE

### **TiO<sub>2</sub> Films with Macroscopic Chiral Nematic-Like Structure Stabilized by Copper Promoting Light-Harvesting Capability for Hydrogen Generation**

Wang, Cong; Mouchet, Sébastien R.; Deparis, Olivier; Li, Jingwei; Paineau, Erwan; Dragoe, Diana; Remita, Hynd; Ghazzal, Mohamed Nawfal

*Published in:*  
Small : nano, micro

*DOI:*  
[10.1002/smll.202402211](https://doi.org/10.1002/smll.202402211)

*Publication date:*  
2024

*Document Version*  
Publisher's PDF, also known as Version of record

[Link to publication](#)

*Citation for published version (HARVARD):*  
Wang, C, Mouchet, SR, Deparis, O, Li, J, Paineau, E, Dragoe, D, Remita, H & Ghazzal, MN 2024, 'TiO<sub>2</sub> Films with Macroscopic Chiral Nematic-Like Structure Stabilized by Copper Promoting Light-Harvesting Capability for Hydrogen Generation', *Small : nano, micro*, vol. 20, no. 42, 2402211. <https://doi.org/10.1002/smll.202402211>

#### **General rights**

Copyright and moral rights for the publications made accessible in the public portal are retained by the authors and/or other copyright owners and it is a condition of accessing publications that users recognise and abide by the legal requirements associated with these rights.

- Users may download and print one copy of any publication from the public portal for the purpose of private study or research.
- You may not further distribute the material or use it for any profit-making activity or commercial gain
- You may freely distribute the URL identifying the publication in the public portal ?

#### **Take down policy**

If you believe that this document breaches copyright please contact us providing details, and we will remove access to the work immediately and investigate your claim.

# TiO<sub>2</sub> Films with Macroscopic Chiral Nematic-Like Structure Stabilized by Copper Promoting Light-Harvesting Capability for Hydrogen Generation

Cong Wang, Sébastien R. Mouchet, Olivier Deparis, Jingwei Li, Erwan Paineau, Diana Dragoë, Hynd Remita, and Mohamed Nawfal Ghazzal\*

Cellulose nanocrystals (CNCs) have inspired the synthesis of various advanced nanomaterials, opening opportunities for different applications. However, a simple and robust approach for transferring the long-range chiral nematic nanostructures into TiO<sub>2</sub> photocatalyst is still fancy. Herein, a successful fabrication of freestanding TiO<sub>2</sub> films maintaining their macroscopic chiral nematic structures after removing the CNCs biotemplate is reported. It is demonstrated that including copper acetate in the sol avoids the epitaxial growth of the lamellar-like structure of TiO<sub>2</sub> and stabilizes the chiral nematic structure instead. The experimental results and optical simulation demonstrate an enhancement at the blue and red edges of the Fabry-Pérot reflectance peak located in the visible range. This enhancement arises from the light scattering effect induced by the formation of the chiral nematic structure. The nanostructured films showed 5.3 times higher performance in the photocatalytic hydrogen generation, compared to lamellar TiO<sub>2</sub>, and benefited from the presence of copper species for charge carriers' separation. This work is therefore anticipated to provide a simple approach for the design of chiral nematic photocatalysts and also offers insights into the electron transfer mechanisms on TiO<sub>2</sub>/Cu<sub>x</sub>O with variable oxidation states for photocatalytic hydrogen generation.

## 1. Introduction

Photoactive structured materials have attracted wide attention in the last few years and have demonstrated promising light-harvesting capability for hydrogen generation.<sup>[1]</sup> Chiral materials, as novel functional materials, have numerous potential applications in sensors, enantiomeric separation, and optoelectronic devices, with their fascinating chemical and physical properties attracting considerable attention.<sup>[2-5]</sup> The transfer of chiral nanostructure into metal oxides is among the most challenging and promising strategies for developing new catalysts. A blatant example is chiral photonic structures, which are often reported as being responsible for the structural coloration of many insects and other biological living species.<sup>[6-11]</sup> In this case, chirality also plays a key role in light-harvesting properties during photosynthesis,<sup>[12]</sup> since it participates in multiple and complex

C. Wang, J. Li, H. Remita, M. N. Ghazzal  
Université Paris-Saclay  
UMR 8000 CNRS  
Institut de Chimie Physique  
Orsay 91405, France  
E-mail: [mohamed-nawfal.ghazzal@universite-paris-saclay.fr](mailto:mohamed-nawfal.ghazzal@universite-paris-saclay.fr)

S. R. Mouchet, O. Deparis  
Department of Physics, and Namur Institute of Structured Matter (NISM)  
University of Namur  
Rue de Bruxelles 61, Namur 5000, Belgium

S. R. Mouchet  
School of Physics  
University of Exeter  
Stocker Road, Exeter EX4 4QL, UK

J. Li  
School of Materials Science and Engineering  
Sun Yat-sen University  
Guangzhou 510275, China

E. Paineau  
Université Paris-Saclay  
UMR 8502 CNRS  
Laboratoire de Physique du Solide  
Orsay 91405, France

D. Dragoë  
Université Paris-Saclay, CNRS  
Institut de Chimie Moléculaire d'Orsay  
Orsay 91405, France

 The ORCID identification number(s) for the author(s) of this article can be found under <https://doi.org/10.1002/sml.202402211>

© 2024 The Author(s). Small published by Wiley-VCH GmbH. This is an open access article under the terms of the [Creative Commons Attribution-NonCommercial](https://creativecommons.org/licenses/by-nc/4.0/) License, which permits use, distribution and reproduction in any medium, provided the original work is properly cited and is not used for commercial purposes.

DOI: 10.1002/sml.202402211

steps, including charge and energy transfer from the organic antenna to active sites. From this perspective, transferring such a kind of nanostructure in photoactive inorganic material is among the most challenging but promising strategies for improving the properties of catalysts for energy applications.<sup>[12–14]</sup> It is, therefore, necessary to have a suitable system that imparts chirality to the final material.

Cellulose nanocrystals (CNCs) are natural materials capable of self-assembly, forming chiral nematic structures in solid films.<sup>[15]</sup> The solubility and stability endow the use of CNCs as biotemplates, transferring the chiral nematic structure to metal oxide films and providing them with photonic properties.<sup>[16]</sup> Thus, SiO<sub>2</sub> with photonic structure was first proposed using a facile and easy one-step method that allowed tuning the photonic properties of silica films.<sup>[17]</sup> However, transferring such structures to other metal transition oxides, such as TiO<sub>2</sub>, has faced multiple challenges. The low stability of titanium precursors (such as chlorides or alkoxides) to moisture enables only the generation of mesoporous TiO<sub>2</sub>, where no chiral nematic structure was observed.<sup>[18–23]</sup> As an alternative, impregnation and hard template methods were proposed to obtain nanostructured TiO<sub>2</sub> films with chiral nematic structures.<sup>[24]</sup> Still, these approaches usually require successive impregnation/drying/etching/calcination steps to get the target films.<sup>[25]</sup> Another way is to use stable precursors to elaborate a photonic hybrid CNCs/TiO<sub>2</sub> films retaining the chiral nematic structure as shown recently.<sup>[26,27]</sup> However, the calcination step required to remove the CNCs biotemplate leads to the formation of 2D lamellar structures at the expense of the chiral nematic structure. In our previous study, we reported that adding Cu as a cocatalyst could stabilize the chiral-like structure in black-TiO<sub>2</sub>.<sup>[28]</sup>

In this work, we aimed to explore the effect of Cu acting as stabilizing the structure, which enhances light harvesting and promotes the photogenerated charge carriers' generation leading to improved photocatalytic H<sub>2</sub> generation. The self-assembly approach requires the use of CNCs biotemplate in the presence of copper (Cu(OAc)<sub>2</sub>) and titanium oxide (Ti(acac)<sub>2</sub>(OiPr)<sub>2</sub>, TAA) precursors in the stock solution. After removing the CNC templates, the TiO<sub>2</sub> films retain their chiral nematic-like structure, observable through the cross-section by scanning electron microscopy. The key compound proved to be the presence of copper. The copper serves as a stabilizer for chiral nematic structures and prevents the sintering during the crystal growth of the TiO<sub>2</sub>. Consequently, the chiral nematic-like structure is maintained at the expense of the lamellar one. Using theoretical optical simulation, we confirmed the beneficial effect of the chiral nematic-like structure in light harvesting properties for hydrogen production. The substantial improvement in photoactivity is attributed to the unique combination of photonic chiral nematic structures and the presence of copper.

## 2. Results and Discussion

The one-pot route used to synthesize the films with a chiral nematic-like structure (referred to as CNTiO<sub>2</sub>/Cu<sub>x</sub>O) is depicted in **Figure 1a**. The starting aqueous CNC suspension (4 wt.%, pH ≈ 6) exhibits birefringence due to the spontaneous self-organization of CNCs into organized chiral nematic structures, as shown in **Figure 1b**. The typical fingerprint is recognized by

the alternated dark and bright lines appearing in the image obtained using a polarized optical microscope (POM). The suspension was mixed with ethanolic TAA solution (0.6 mL of TAA in 2 mL ethanol) and variable volume of ethanolic Cu(OAc)<sub>2</sub> solutions to form transparent yellow-green mixtures (**Figure 1c**; **Table S1**, Supporting Information). The addition of TAA and Cu(OAc)<sub>2</sub> solutions lowers the concentration of the stock solution, turning the anisotropic phase into isotropic, as demonstrated by the dark image under POM (**Figure 1c**). Subsequently, the mixture was poured into polystyrene Petri dishes, allowing the solvent evaporation to induce the self-assembly of CNCs to form solid CNC/TiO<sub>2</sub>/Cu(OAc)<sub>2</sub> hybrid films. Iridescent colors can be observed after approximately two days of drying, indicating the formation of photonic structures (**Figure 1d**).<sup>[29]</sup>

A typical fingerprint with alternating bright and dark lines is observed under POM observation, attesting to the formation of CN ordering in the hybrid films (**Figure 2a**; **Figure S1**, Supporting Information). The removal of CNCs templates was achieved by calcination at 500 °C in air. The resulting freestanding films display a light tawny color with strong birefringence and distinctive fingerprint patterns under POM (**Figure 2b**; **Figure S2**, Supporting Information), confirming that the CN-like structure is preserved after the calcination step. These films exhibit a Bragg reflection peak with maximum reflectance spectra at ≈450 nm (**Figure 2c**). Interestingly, the increase in the amount of Cu(OAc)<sub>2</sub> induces a slight red-shift in the maximum of the Bragg peak, corresponding to an increase in the pitch of the chiral nematic structure of the films. The shift was found to be higher at lower loading of copper acetate. However, over 0.1 wt.%, the observed redshift is limited to a few nanometers compared to lower values of copper acetate, which could be due to the interaction between Cu<sup>2+</sup> with sulfates function at the surface of cellulose nanocrystals.

The difference in the films' structures before and after calcination was revealed through scanning electron microscopy (SEM). Cross-section SEM images of CNC/TiO<sub>2</sub> hybrid films show periodic left-handed twisting that is repeated along the direction normal to the film (plane/surface), confirming the existence of CN structures (**Figure 3a**). The distance between two twisted layers corresponds to half of the helical pitch (*P*). The introduction of Cu(OAc)<sub>2</sub> does not interfere with the organization of CNCs since the CN structures are still clearly visible in hybrid films (**Figure 3b,c**). The result demonstrated that the optimal range of copper acetate is 0.05–0.8 wt.%. In fact, above this range, which fastens the sol-gel transition, leading to gel formation. It is worth noting that adding a higher copper acetate concentration leads to strong crosslinking between Cu<sup>2+</sup> and sulfated cellulose nanocrystals which fastens the sol-gel transition, leading to gel formation. As we previously reported, calcination can effectively remove the CNCs template from the CNC/TiO<sub>2</sub> composite and allow obtaining the photoactive anatase phase of TiO<sub>2</sub>.<sup>[13]</sup> The copper-free films show a lamellar structure of the TiO<sub>2</sub> films (LTiO<sub>2</sub>) due to the crystal growth and sintering (**Figure 3d,e**), in agreement with our previous work.<sup>[13]</sup> Copper-containing films, on the other hand, show that well-defined CN-like structures still can be observed after calcination (**Figure 3f–i**; **Figure S3**, Supporting Information), similar to the morphology of the hybrid CNTiO<sub>2</sub>/Cu<sub>x</sub>O films before calcination (**Figure 3b,c**). The film features a long-range ordered layers and twisted-like morphology reminiscent of the chiral nematic structure. Cu is mixed with

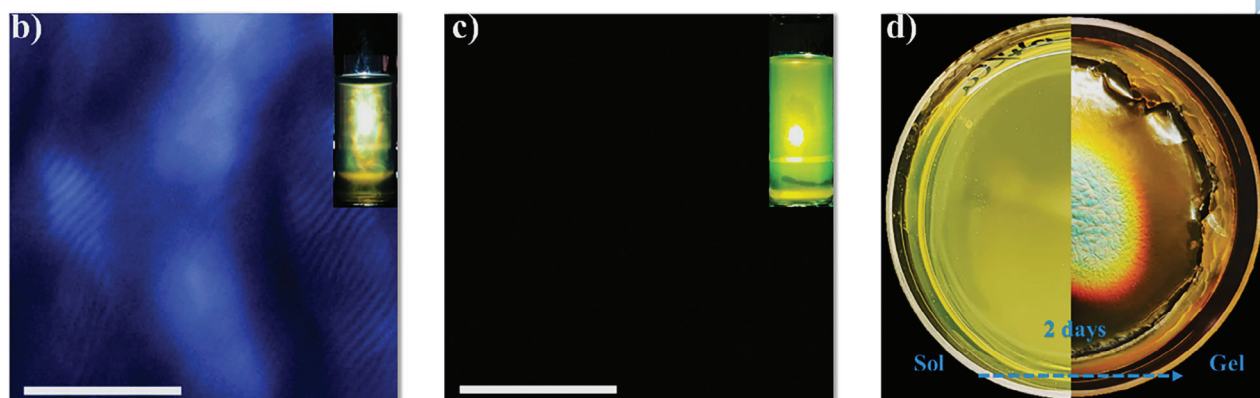
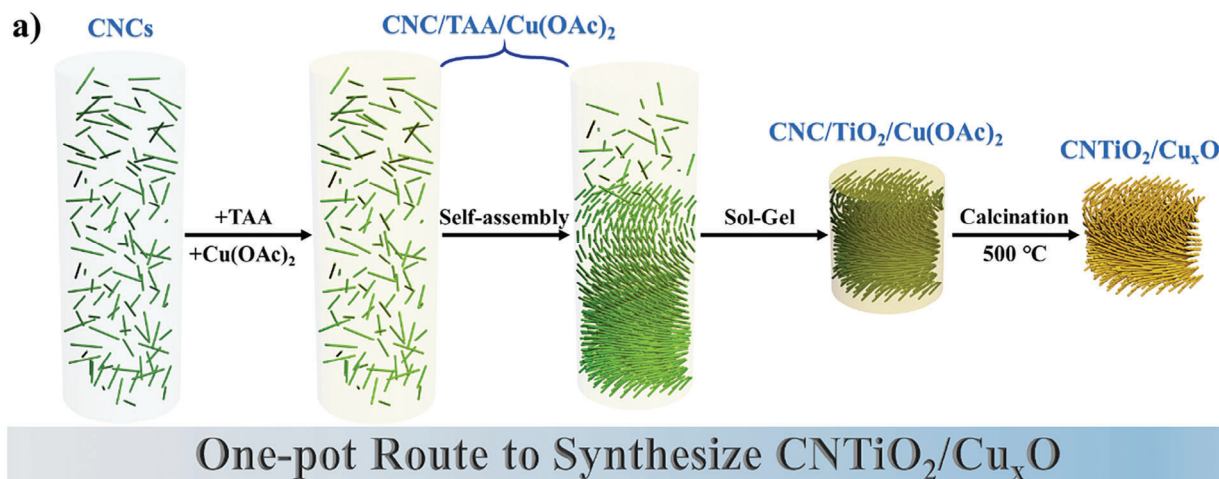


**Figure 1.** a) Schematic illustration of the chiral nematic freestanding TiO<sub>2</sub>/Cu<sub>x</sub>O film synthesis. POM images and photographs (under polarized light) of b) 4 wt.% CNCs suspension and c) CNC/TAA/Cu(OAc)<sub>2</sub> solution. The insets represent macroscopic optical observations between crossed polarizers. d) Photographs of the sol-gel process of CNC/TAA/Cu(OAc)<sub>2</sub> solution for 2 days at room temperature.

the TiO<sub>2</sub>, forming a homogenous film as evidenced in Figure S4 (Supporting Information).<sup>[26]</sup> In addition, it appears that copper inhibits the sintering of the TiO<sub>2</sub> crystal during the calcination step, avoiding the formation of the lamellar structure. Indeed, Cu is reported to lower the temperature of crystallization of TiO<sub>2</sub>, which can reduce the surface energy and hinder the sintering observed for copper-free films.<sup>[30]</sup> However, at higher concentrations of copper acetate, the films do not exhibit any visible ordered structure. Instead, as shown in Figure S5 (Supporting Information), the chiral nematic structure is destroyed and replaced by a porous film. The copper acetate precursor due to the charge of the Cu<sup>2+</sup> cations has the potential to disrupt the formation of the chiral nematic structure and cause gelation before/during drying due to charge-balancing effects.

X-ray scattering (XRS) was performed to characterize the structure of the samples and their related crystallinity form. CNC/TiO<sub>2</sub>/Cu(OAc)<sub>2</sub> hybrid films showed several characteristic peaks at  $Q \approx 1.1 \text{ \AA}^{-1}$   $[[1\bar{1}0], (110)]$  and  $1.6 \text{ \AA}^{-1}$  (200) corresponding to the crystalline structure of *I<sub>h</sub>* cellulose form.<sup>[31]</sup> After the calcination of the films, all the samples present the characteristic peaks related to anatase TiO<sub>2</sub> (Figure 4a). No diffraction peaks associated with Cu species were observed due to the low quantity of Cu loading (<0.8 wt.%), below the detection sensitivity.<sup>[32]</sup> There

was no alteration in the crystalline structure, but a slight decrease in the crystal size of anatase TiO<sub>2</sub> was observed. The size of TiO<sub>2</sub> crystallites decreased by  $\approx 1 \text{ nm}$  as the Cu loading increased from 0 to 0.8 wt.% (Table S2, Supporting Information), in agreement with the fact that Cu limits the crystal growth of TiO<sub>2</sub>.<sup>[30]</sup> Furthermore, doping with Cu can inhibit the transformation of TiO<sub>2</sub> from anatase to a more compact rutile form during the calcination process, thereby improving the phase stability of the TiO<sub>2</sub> and favoring the preservation of the CN structures.<sup>[32]</sup> Low- and high-resolution transmission electron microscopy (HRTEM) was employed to offer further insight into the microstructure of CNTiO<sub>2</sub>/Cu<sub>0.4%</sub>, confirming the doping of Cu into the TiO<sub>2</sub> lattice (Figure 4b; Figure S6, Supporting Information). The crystalline sizes of TiO<sub>2</sub> observed in HRTEM images were comparable to those deduced from the XRS patterns. The crystal lattice constants were identified to be 3.5, 2.06, 2.16, 2.4, and 2.53 Å corresponding to the anatase TiO<sub>2</sub> (101), metallic Cu (111), cubic phase Cu<sub>2</sub>O (200), monoclinic phase CuO (111) and (002), respectively. Noticeably, the interfaces between TiO<sub>2</sub> and various Cu species were physically in contact and potentially formed different junctions (including Cu/TiO<sub>2</sub> Schottky junction, Cu<sub>2</sub>O/TiO<sub>2</sub> p-n junction, and CuO/TiO<sub>2</sub> heterojunction). The presence of CuO was analyzed in an electron diffraction (ED) pattern

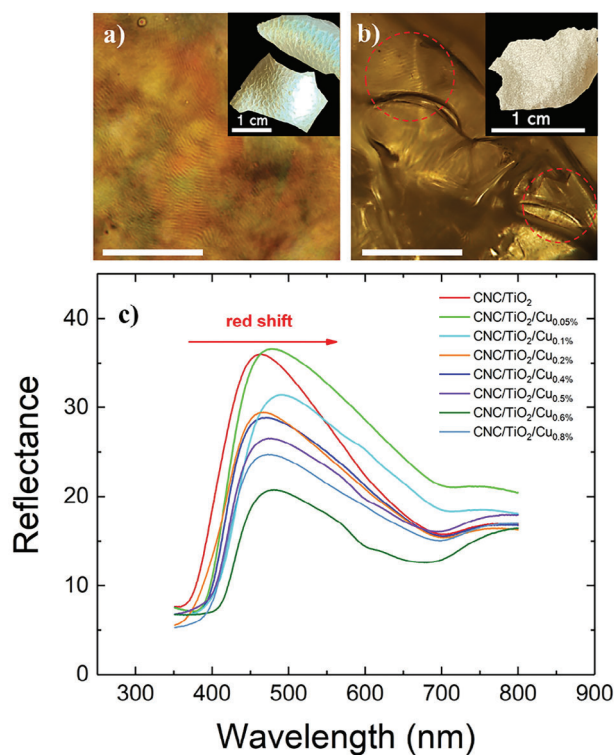


**Figure 2.** POM images and photographs of a) CNC/TiO<sub>2</sub>/Cu(OAc)<sub>2</sub> hybrid film and b) freestanding CNTiO<sub>2</sub>/Cu<sub>x</sub>O film (the mass loading of Cu is 0.4%). All scale bars correspond to 50 μm. c) Reflectance spectra of the hybrid films obtained with variable amounts of copper.

(inset in Figure 4b).<sup>[33]</sup> This finding echoed the results from XRS, in which no diffraction peaks associated with Cu species except those of anatase TiO<sub>2</sub> were detected. Energy-dispersive X-ray spectroscopy (EDS) mapping in scanning transmission electron microscopy by using a high-angle annular dark-field detector (STEM-HAADF) showed the homogeneous dispersion of Cu species in CNTiO<sub>2</sub>/Cu<sub>x</sub>O films (Figure S6, Supporting Information).

The optical properties of as-prepared films were analyzed by UV-vis diffuse reflectance spectra (DRS) (Figure 5a). The absorption in the UV region is assigned to the band-to-band transition of TiO<sub>2</sub>.<sup>[34]</sup> The LTiO<sub>2</sub> showed a noticeable enhancement in light absorption compared to TiO<sub>2</sub>-P25 due to multiple light scattering caused by the lamellar structure (Figure 5a).<sup>[13]</sup> Introducing Cu further improves light absorption capability in the visible region (400–800 nm wavelength). It extends the absorption edges, ascribed to Cu 3d–Ti 3d optical transition formation.<sup>[35]</sup> The absorption was enhanced with the increase in Cu loading, while the rising trend essentially saturated above 0.4 wt.% Cu. In addition, an extra broad band ≈750 nm corresponding to the d–d transition of Cu was observed (Figure 5a).<sup>[36]</sup> The bandgaps ( $E_g$ ) of CNTiO<sub>2</sub>/Cu<sub>x</sub>O films were estimated from Kubelka–Munk (K-M) theory. In agreement with the absorption measurement, LTiO<sub>2</sub> exhibited a narrower bandgap (3.0 eV) than TiO<sub>2</sub>-P25 (3.2 eV) and a reduction from 3.0 to 2.7 eV in the bandgap of CNTiO<sub>2</sub>/Cu<sub>x</sub>O was noticed with the addition of Cu (Figure 5b). The coupling of TiO<sub>2</sub> anatase to Cu<sub>x</sub>O, which is reported to have a smaller

bandgap, leads to the reduction of the electronic bandgap of the nanocomposite. Indeed, Cu doping of TiO<sub>2</sub> lattice could introduce intermediate states that reduce bandgap.<sup>[37]</sup> To provide further insight into the effect of the chiral nematic-like structure on the absorptance properties, we numerically simulated the absorptance of the films. The simulations were performed at normal incidence using a one-dimensional Berreman 4 × 4 matrix method for stratified anisotropic media,<sup>[38–40]</sup> applying Jones calculus to account for light propagation through the chiral nematic multilayered structure, and the results are shown in Figure 5c.<sup>[41]</sup> Such a matrix formalism enables the propagation of the solution across the layers. Essentially, the electromagnetic fields' continuity conditions at the interfaces of adjacent layers are represented through matrix equations. This yields a transfer matrix for traversing the interface. By sequentially multiplying these matrices, the solution propagates all through the layers, providing the structure's reflectance and transmittance. This approach is straightforward and generally yields accurate results. Consequently, it has been recurrently used to model electromagnetic wave propagation in layered media in general and, specifically, in nematic structures, including CNC films.<sup>[42–44]</sup> The helicoidal structure was treated as a stack of birefringent layers with a 219-nm pitch on an isotropic, lossless, and non-dispersive substrate with a refractive index (RI) of 1.50. The incidence medium was chosen to be air. The ordinary RI  $n_o(\lambda)$  and  $k_o(\lambda)$  of Cu-TiO<sub>2</sub> between 400 and 900 nm were taken from ref.[41] where the material was annealed at 500 °C.<sup>[45]</sup> In the absence of published data in the UV range, values of  $n_o(\lambda)$  and  $k_o(\lambda)$  in the 200–400 nm range were assumed to be constant and equal to  $n_o(\lambda = 400 \text{ nm}) = 2.83$  and 1.60, respectively, to account for the bandgap at ca. 3.1 eV. We accounted for birefringence by assuming the extraordinary RI  $n_e(\lambda) = n_o(\lambda) - 0.3$  and  $k_e(\lambda) = k_o(\lambda) - 0.01$ . The absorptance and reflectance were averaged over transverse magnetic (TM) and transverse electric (TE) polarizations, i.e., simulating unpolarized incident light. Our simulations show an enhancement of absorptance  $A_{av}$  at the blue and red edges of the Fabry-Pérot reflectance peak located at 465 nm with respect to a non-chiral birefringent 219-nm-thin film with the same RI (Figure 5c). This enhancement arises from the slow photon effect, previously reported in other contexts.<sup>[46,47]</sup> With an increasing number of pitches in the photonic structure, a Bragg reflectance peak appears in the spectra at ca. 600 nm due to the formation of a multilayer stack (Figure S7, Supporting Information). Some absorptance enhancement at the edges of Bragg peaks is observed akin to the one-pitch structure of Figure 5c. Guided by such simulations, the chiral nematic structures can be tuned to enhance photocatalysis by decreasing the pitch to position the red edge of the Bragg reflectance peak close to the electronic absorption band edge of the photocatalyst.<sup>[48,49]</sup> This optimization in band structure arose from incorporating Cu, which could produce a donor level below the conduction band (CB) of TiO<sub>2</sub> and enhance light absorption. Moreover, incorporating Cu contributed to modifying the electronic density of states and promoting the charge separation of TiO<sub>2</sub>, endowing the CNTiO<sub>2</sub>/Cu<sub>x</sub>O films with great potential in photocatalysis.<sup>[50]</sup>

The photocatalytic properties of CNTiO<sub>2</sub>/Cu<sub>x</sub>O films are evaluated for hydrogen evolution reaction (HER). The HER experiment used triethanolamine (TEOA) as a sacrificial electron donor to evaluate the photocatalytic activity of the CNTiO<sub>2</sub>/Cu<sub>x</sub>O films

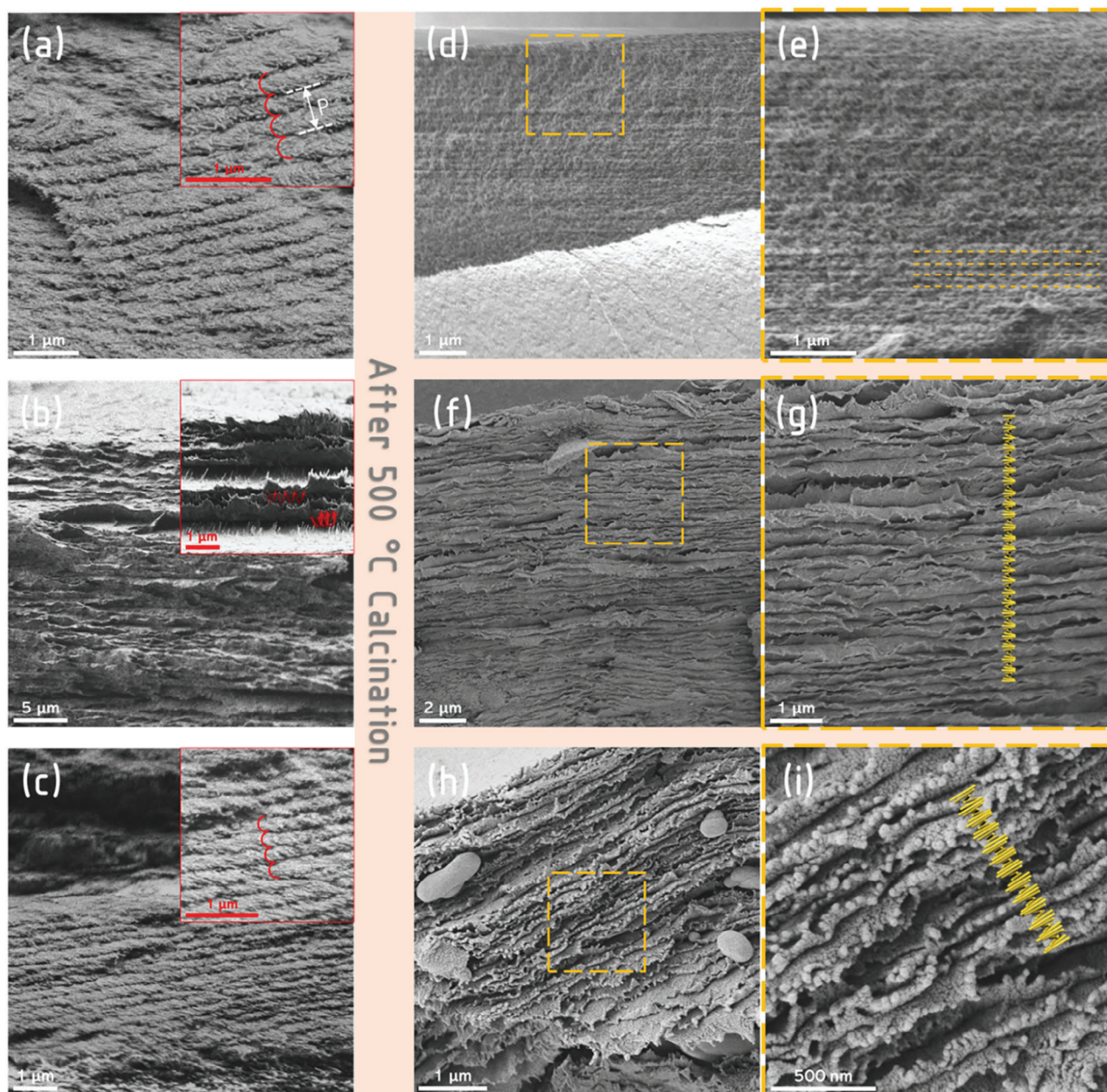


**Figure 3.** Cross-section SEM images of composite films prior to and after calcination. a) CNC/TiO<sub>2</sub> hybrid film, b) CNC/TiO<sub>2</sub>/Cu<sub>0.2%</sub> hybrid film, c) CNC/TiO<sub>2</sub>/Cu<sub>0.4%</sub> hybrid film, d,e) LTiO<sub>2</sub> film, f,g) CNTiO<sub>2</sub>/Cu<sub>0.2%</sub> calcined films and (h,i) CNTiO<sub>2</sub>/Cu<sub>0.4%</sub> calcined films.

with different Cu mass loadings (Figure 6a). The LTiO<sub>2</sub> showed an enhanced photocatalytic H<sub>2</sub> evolution rate compared to commercial TiO<sub>2</sub>-P25. By introducing a very small amount of Cu (0.05 wt.%), the production rate of CNTiO<sub>2</sub>/Cu<sub>0.05%</sub> remarkably increased, reaching a rate of 0.28 mmol g<sup>-1</sup> h<sup>-1</sup>, 5.3 times higher than that of TiO<sub>2</sub>. The highest H<sub>2</sub> evolution rate of 0.73 mmol g<sup>-1</sup> h<sup>-1</sup> was reached by CNTiO<sub>2</sub>/Cu<sub>0.4%</sub>. The optimal photocatalytic activity is in agreement with the evolution of the absorbance obtained from UV-vis absorption spectra. Further increase in the Cu loading up to 0.8 wt.% leads to a decrease in the photocatalytic activity of CNTiO<sub>2</sub>/Cu<sub>x</sub>O films, which could be attributed to the partial blocking of active TiO<sub>2</sub> caused by the growth of

Cu<sub>x</sub>O particles at higher loading.<sup>[51]</sup> An alternative interpretation is that excess Cu could serve as recombination sites shortening the photogenerated charge carriers' lifetime, which results in a lower H<sub>2</sub> evolution rate.<sup>[52]</sup> The optimized CNTiO<sub>2</sub>/Cu<sub>0.4%</sub> exhibited excellent stability without any significant decrease in the photocatalytic activity during five successive cycles (Figure 6b).

To obtain further insight into the mechanism of the photocatalytic H<sub>2</sub> reaction, electrochemical impedance spectroscopy (EIS) was measured to assess the electric charge transfer resistances of CNTiO<sub>2</sub>/Cu<sub>x</sub>O films. The smaller the semicircle of the Nyquist plots at low frequencies, the higher the charge transfer

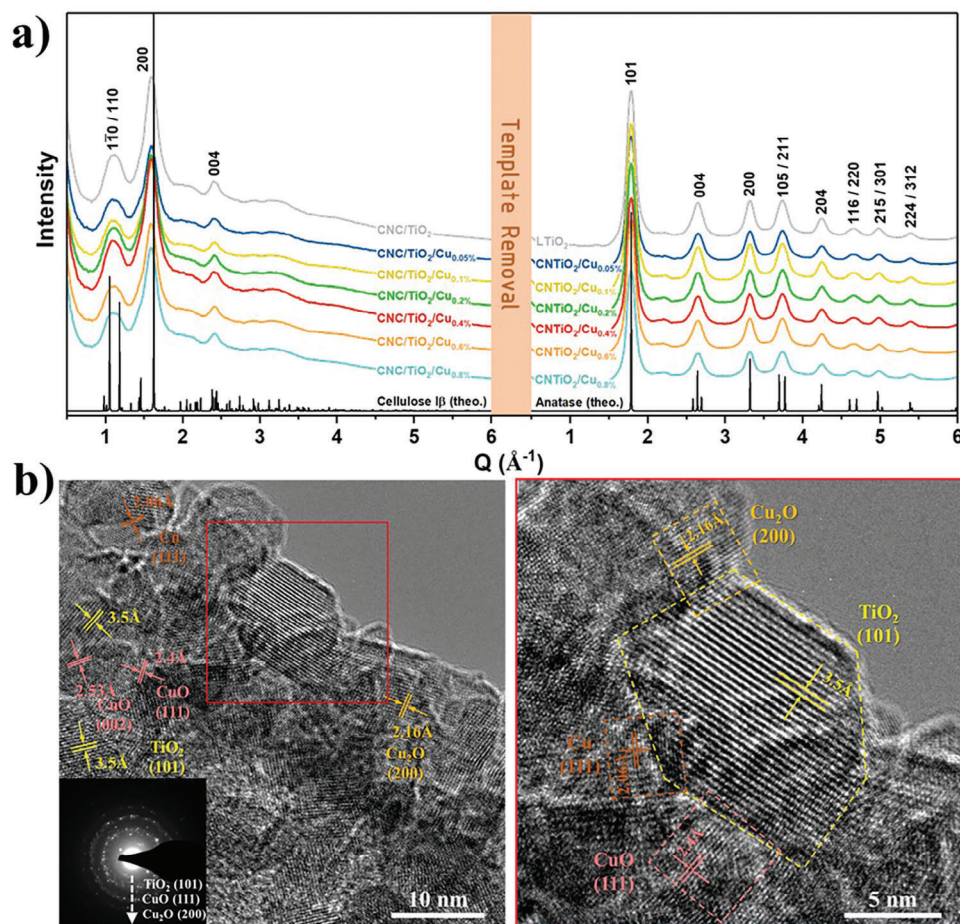


**Figure 4.** a) XRD patterns of CNC/TiO<sub>2</sub> and CNC/TiO<sub>2</sub>/Cu hybrid films, and the XRD patterns of LTiO<sub>2</sub> and CNTiO<sub>2</sub>/Cu<sub>x</sub>O photonic films after removing CNCS template. b) HRTEM images of CNTiO<sub>2</sub>/Cu<sub>0.4%</sub>.

ability at the catalyst/electrolyte interface (Figure S8a, Supporting Information).<sup>[53]</sup> A significant reduction of the semi-circle radius was observed in CNTiO<sub>2</sub>/Cu<sub>x</sub>O films compared to LTiO<sub>2</sub>, crediting to the formation of heterojunction between TiO<sub>2</sub> and Cu<sub>x</sub>O, which can enhance the electrical conductivity and charge transfer efficiency.<sup>[54]</sup> Among all samples, CNTiO<sub>2</sub>/Cu<sub>0.4%</sub> showed the best charge transfer ability. Accordingly, the transient photocurrent response of CNTiO<sub>2</sub>/Cu<sub>x</sub>O films exhibits the same increasing trend in photocurrent intensity, suggesting efficient carriers' separation under light irradiation (Figure S8b, Supporting Information). Time-resolved studies show that electrons are transferred from TiO<sub>2</sub> to Cu<sub>x</sub>O (Figure S8c, Supporting Information), in agreement with EIS and PEC results. The CNTiO<sub>2</sub>/Cu<sub>x</sub>O photocatalyst underwent a distinct photoactivation process during the photocatalytic HER cycle. Noticeably, we observed a color change of CNTiO<sub>2</sub>/Cu<sub>x</sub>O photocatalyst during the reaction from white, dark grey to black with increasing H<sub>2</sub> bubbles after one hour of UV-vis irradiation, which originated from the local distortion of TiO<sub>2</sub> lattice caused by the electrons trapped in the Cu d-orbitals (Figure 6c).<sup>[36]</sup> This black color gradually reverted to the original white after several hours of exposure to the air under dark conditions, corresponding to a complete photoactivation cycle.<sup>[55]</sup> To further explore the origin of the H<sub>2</sub> evolution reac-

tivity of CNTiO<sub>2</sub>/Cu<sub>x</sub>O during the photoactivation process, the black-activated photocatalyst was collected under argon flow and analyzed by X-ray photoelectron spectroscopy (XPS). The general XPS surveys of CNTiO<sub>2</sub>/Cu<sub>x</sub>O before and after calcination, and before and after activation indicated the presence of Cu, Ti, C, and O species (Figure S9, Supporting Information). The high-resolution XPS of the films before and after calcination are shown in Figure S10 (Supporting Information). The results indicate the presence of titanium dioxide and Cu 2p in its Cu<sup>2+</sup> oxidation state, as indicated by the satellite present in the spectrum. The high-resolution XPS spectra of Cu 2p in original CNTiO<sub>2</sub>/Cu<sub>x</sub>O showed peaks with binding energy (BE) at 952.4 and 932.6 eV, which were ascribed to Cu<sup>+</sup>, while the ones located at 953.3 and 933.6 eV could be attributed to Cu<sup>2+</sup> (Figure 6d). The existence of a broad satellite peak further confirmed the presence of Cu<sup>2+</sup>.<sup>[54]</sup> Cu<sup>0</sup> was also present, even if it was difficult to distinguish due to its low content and the overlap of the binding energy with Cu<sup>+</sup>.<sup>[56]</sup> In comparison, the peaks and satellite peaks corresponding to Cu<sup>2+</sup> were eliminated and replaced by the peaks attributed to Cu<sup>+</sup>/Cu after light excitation, suggesting a reduction of Cu<sup>2+</sup> triggered by the electrons generated from TiO<sub>2</sub>. Relatively, a slight shift toward lower binding energy accompanied by the appearance of a peak centered at 462.7 eV assigned to Ti<sup>3+</sup> was also

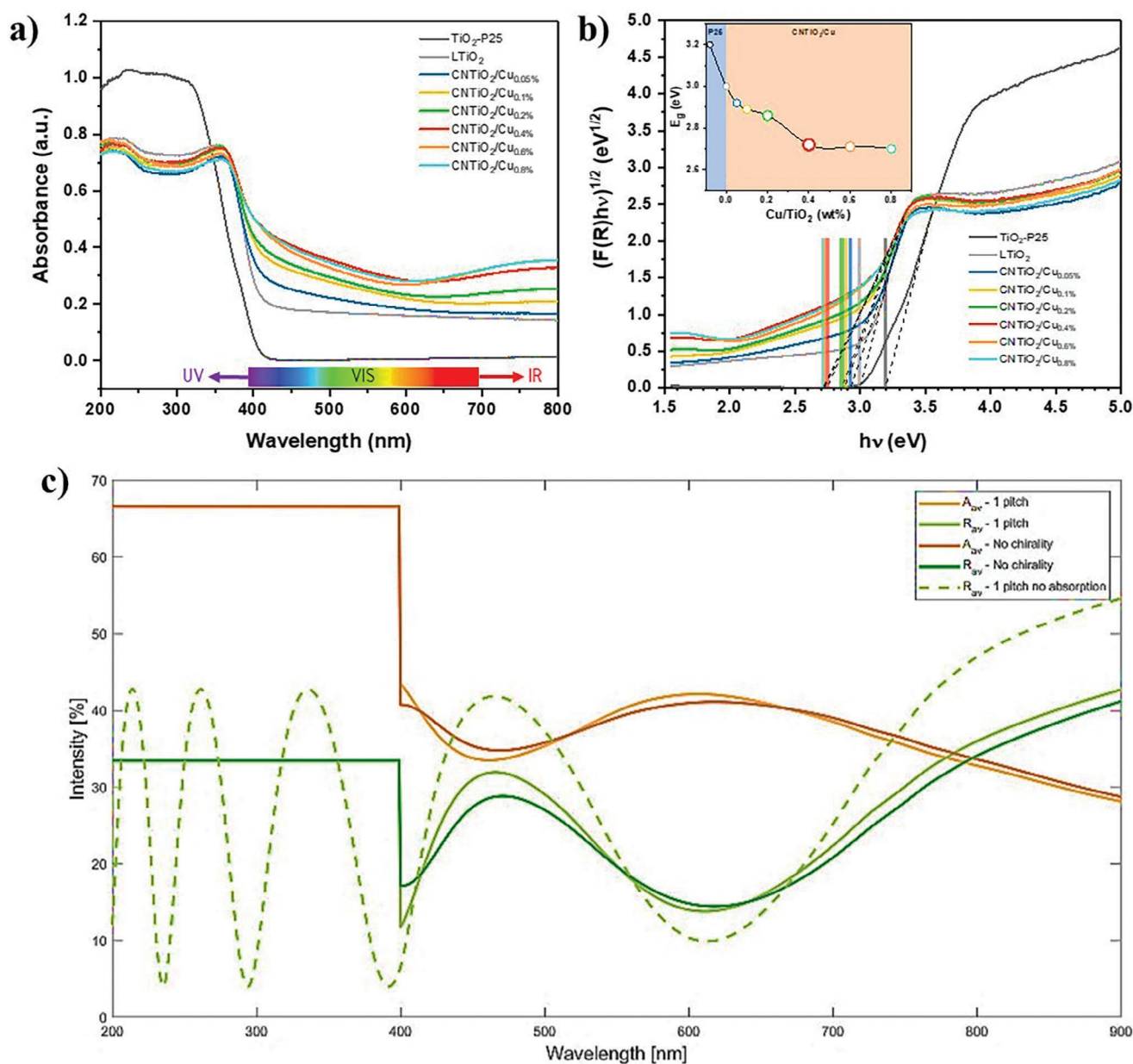


**Figure 5.** a) UV-vis absorption spectra and b) the corresponding Kubelka–Munk plot of  $\text{TiO}_2$ -P25,  $\text{LTiO}_2$ , and  $\text{CNTiO}_2/\text{Cu}_x\text{O}$  photonic films. The Inset in b) is the evolution of the optical bandgap with different Cu loadings. Simulated absorbance and reflectance spectra c) of a one-pitch chiral thin film agree with the experimental observations in a) and (Figure 2c), respectively. Absorbance ( $A_{av}$ ) and reflectance ( $R_{av}$ ) spectra (averaged over TM and TE polarizations) of such a chiral film are compared to the ones from a non-chiral birefringent film of identical thickness. The reflectance spectrum of a one-pitch chiral thin film without absorption ( $k_e(\lambda) = k_o(\lambda) = 0.00$ , dashed curve) allows one to locate accurately the red and blue edges of the reflectance peak.

observed in activated photocatalysis.<sup>[57]</sup> The change in the oxidation state of Cu species can rationalize the color change from white to dark. The light excitation generates electrons in the conduction band of  $\text{TiO}_2$ , which are transferred to copper and reduce  $\text{Cu}^{2+}$  to  $\text{Cu}^+$  and  $\text{Cu}^0$ . After the exposure of the photocatalyst to air, a reverse oxidation of copper leads to recovering the original color. Based on the characterization results, a photocatalytic mechanism for  $\text{CNTiO}_2/\text{Cu}_x\text{O}$  films during the photoactivation cycle can be proposed (Figure 6e). Initially, the

$\text{CNTiO}_2/\text{Cu}_x\text{O}$  photocatalyst is inactive (S0), which could change to the excited state (S1) through light excitation and simultaneously generate  $e^-/h^+$  pairs. Immediately posterior, the photo-generated electrons ( $e^-$ ) transfer from  $\text{Cu}_2\text{O}$  (CB) to  $\text{TiO}_2$  (CB) through the p-n junction and then from  $\text{TiO}_2$  to the d-orbital of metallic Cu and CuO (S2). On the other hand, the holes ( $h^+$ ) are scavenged by the sacrificial agent. The localization of electrons at Cu species leads to an active state (S3) for HER. In addition, the trapped electrons by copper oxide (CuO) species can reduce

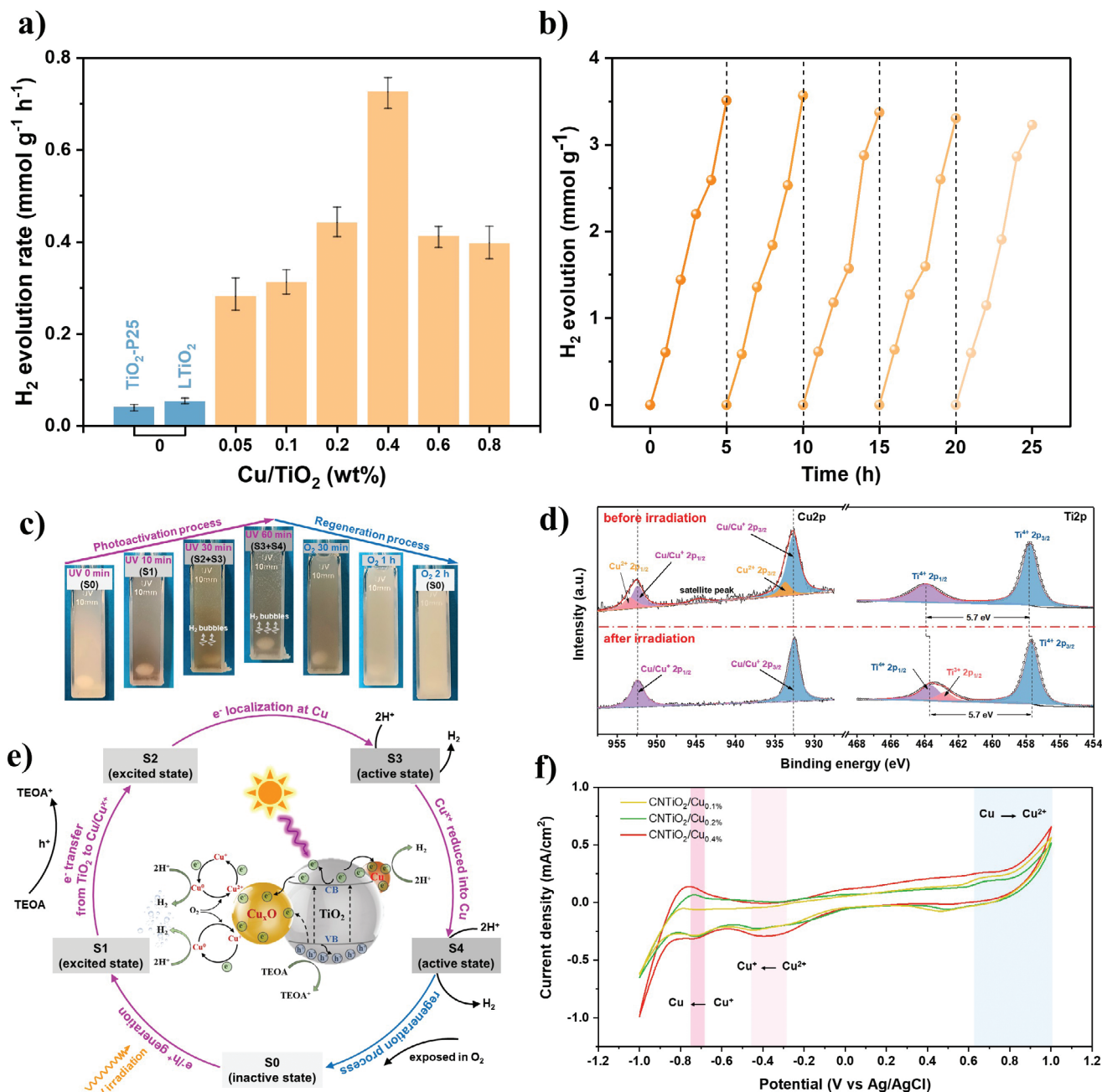


**Figure 6.** a) Kinetic constant of the photocatalytic H<sub>2</sub> evolution reaction of TiO<sub>2</sub>-P25, LTiO<sub>2</sub>, and CNTiO<sub>2</sub>/Cu<sub>x</sub>O films. b) Cycling test obtained for the CNTiO<sub>2</sub>/Cu<sub>0.4%</sub> photocatalysts. c) Photographs of CNTiO<sub>2</sub>/Cu<sub>0.4%</sub> film in various states of photoactivation cycle. d) XPS spectra of Cu 2p before and after UV-vis irradiation. e) Photocatalytic mechanism over CNTiO<sub>2</sub>/Cu<sub>x</sub>O film during the photoactivation cycle. f) Cyclic voltammograms of CNTiO<sub>2</sub>/Cu<sub>x</sub>O films with different Cu loadings.

Cu<sup>2+</sup> to Cu<sup>+</sup>/Cu<sup>0</sup>, representing highly active sites (S4), resulting in enhanced photoactivity.<sup>[58]</sup> Notably, the active sites (S3 and S4) can gradually return to the original inactive state (S0) after approximately two hours of exposure to the air under dark conditions, i.e., the Cu<sup>+</sup>/Cu<sup>0</sup> was oxidized by O<sub>2</sub> or h<sup>+</sup>. The variable valence states of copper during the photoactivation cycle create additional transfer pathways for the photogenerated electrons, which are beneficial for photocatalytic HER. More importantly,

this CNTiO<sub>2</sub>/Cu<sub>x</sub>O photocatalyst exhibits a reversible interaction between Cu<sub>x</sub>O and the adjacent TiO<sub>2</sub>.

The presence of low-oxidation states of Cu and Ti after illumination was further proved by valence band (VB) XPS spectra (Figure S11, Supporting Information), which was conducive to the higher photocatalytic activity of the CNTiO<sub>2</sub>/Cu<sub>x</sub>O. Moreover, cyclic voltammetry (CV) was applied to investigate the redox ability and the change in the valence state of CNTiO<sub>2</sub>/Cu<sub>x</sub>O. Two

quasi-reversible reduction peaks corresponding to the reduction of  $\text{Cu}^{2+}$  to  $\text{Cu}^+$  and the reduction of  $\text{Cu}^+$  to metallic Cu, respectively, were observed in Figure 6f. Conversely, Cu was stripped and wholly oxidized to  $\text{Cu}^{2+}$  when reaching a higher positive potential.<sup>[59]</sup>  $\text{CNTiO}_2/\text{Cu}_{0.4\%}$  showed relatively lower reduction potentials of  $\text{Cu}^{2+}$  to  $\text{Cu}^+$  ( $-0.38$  V) and  $\text{Cu}^+$  to  $\text{Cu}^0$  ( $-0.72$  V), which is beneficial to the photocatalytic reduction reaction.<sup>[60]</sup>

### 3. Conclusion

In summary, we have successfully synthesized photonic  $\text{TiO}_2/\text{Cu}_x\text{O}$  freestanding films with unique chiral nematic structures using cellulose nanocrystals as bio-templates via a straightforward one-pot chemistry route. The participation of copper oxide species enhances the stability of chiral nematic structures in the  $\text{TiO}_2/\text{Cu}_x\text{O}$  films and simultaneously serves as a co-catalyst for photocatalytic  $\text{H}_2$  evolution reaction. This novel photonic  $\text{TiO}_2/\text{Cu}_x\text{O}$  possesses a synergetic effect in the photocatalysis process: i) the well-preserved chiral nematic nanostructure improves the light-harvesting capability; ii) the co-presence of  $\text{Cu}^{2+}$ ,  $\text{Cu}^+$ , and  $\text{Cu}^0$  provides a variety of pathways for electron transfer, favoring the separation of photogenerated charge carriers. Moreover, the performance stability and electron transfer mechanism of  $\text{TiO}_2/\text{Cu}_x\text{O}$  during the photoactivation cycles are further revealed. The present study explores a simple one-pot route to synthesize distinctive macroscopic chiral nematic-like  $\text{TiO}_2/\text{Cu}_x\text{O}$  photocatalysts and provides insights into the electron transfer during the photoactivation cycle. Finally, numerical predictions of the optical properties of this photonic film showed their potential for the development of photocatalytic applications enhanced by structured photonic structures, not only to understand the underlying optical mechanisms, but also to optimize the design of such structures.

### Supporting Information

Supporting Information is available from the Wiley Online Library or from the author.

### Acknowledgements

C.W. acknowledges the China Scholarship Council (CSC) for his fellow research position. The authors thank Diana Dragoe for the XPS analysis. S.R.M. was supported by a BEWARE Fellowship (Convention n°2110034) of the Walloon Region (CO-FUND Marie Skłodowska-Curie Actions of the European Union #847587), as a Postdoctoral Researcher. The authors thank François Brisset for collecting the SEM images and Paul Haghi-Ashtiani for the TEM images. TEM work was carried out using the facilities available at the MSSMat laboratory within the MATMECA consortium, which is supported by the Agence Nationale de la Recherche (ANR) under contract number ANR-10-EQPX-37.

### Conflict of Interest

The authors declare no conflict of interest.

### Data Availability Statement

The data that support the findings of this study are available from the corresponding author upon reasonable request.

### Keywords

cellulose nanocrystals, copper oxides, photocatalysis, photonic structure, titanium dioxide

Received: March 20, 2024

Revised: May 18, 2024

Published online:

- [1] C. Wang, M. N. Ghazzal, *Energy Adv.* **2023**, 2, 965.
- [2] O. Kose, A. Tran, L. Lewis, W. Y. Hamad, M. J. MacLachlan, *Nat. Commun.* **2019**, 10, 510.
- [3] C. E. Boott, A. Tran, W. Y. Hamad, M. J. MacLachlan, *Angew. Chem. Int. Ed.* **2020**, 59, 226.
- [4] M. Kaushik, K. Basu, C. Benoit, C. M. Cirtiu, H. Vali, A. Moores, *J. Am. Chem. Soc.* **2015**, 137, 6124.
- [5] R. Xiong, J. Luan, S. Kang, C. Ye, S. Singamaneni, V. V. Tsukruk, *Chem. Soc. Rev.* **2020**, 49, 983.
- [6] V. Sharma, M. Crne, J. O. Park, M. Srinivasarao, *Science* **2009**, 325, 449.
- [7] L. T. McDonald, E. D. Finlayson, B. D. Wilts, P. Vukusic, *Interface Focus* **2017**, 7, 20160129.
- [8] E. D. Finlayson, L. T. McDonald, P. Vukusic, *J. R. Soc. Interface* **2017**, 14, 20170129.
- [9] S. Vignolini, P. J. Rudall, A. V. Rowland, A. Reed, E. Moyroud, R. B. Faden, J. J. Baumberg, B. J. Glover, U. Steiner, *Proc. Nat. Acad. Sci.* **2012**, 109, 15712.
- [10] M. Kollé, A. Lethbridge, M. Kreysing, J. J. Baumberg, J. Aizenberg, P. Vukusic, *Adv. Mater.* **2013**, 25, 2239.
- [11] S. R. Mouchet, O. Deparis, *Natural Photonics and Bioinspiration*, Artech House, Norwood, MA **2021**.
- [12] N. Mittal, S. Tien, E. Lizundia, M. Niederberger, *Small* **2022**, 18, 2107183.
- [13] C. Wang, J. Li, E. Paineau, A. Laachachi, C. Colbeau-Justin, H. Remita, M. N. Ghazzal, *J. Mater. Chem. A* **2020**, 8, 10779.
- [14] M. Schreck, R. Deshmukh, E. Tervoort, M. Niederberger, *Chem. Mater.* **2021**, 34, 43.
- [15] J. F. Revol, H. Bradford, J. Giasson, R. H. Marchessault, D. G. Gray, *Int. J. Biol. Macromol.* **1992**, 14, 170.
- [16] E. Dujardin, M. Blaseby, S. Mann, *J. Mater. Chem.* **2003**, 13, 696.
- [17] K. E. Shopsowitz, H. Qi, W. Y. Hamad, M. J. MacLachlan, *Nature* **2010**, 468, 422.
- [18] A. Ivanova, M. C. Fravventura, D. Fattakhova-Rohlfing, J. Rathouský, L. Movsesyan, P. Ganter, T. J. Savenije, T. Bein, *Chem. Mater.* **2015**, 27, 6205.
- [19] A. Ivanova, D. Fattakhova-Rohlfing, B. E. Kayaalp, J. Rathousky, T. Bein, *J. Am. Chem. Soc.* **2014**, 136, 5930.
- [20] J. Xue, F. Song, X.-W. Yin, Z.-L. Zhang, Y. Liu, X.-L. Wang, Y.-Z. Wang, *ACS Sustainable Chem. Eng.* **2017**, 5, 3721.
- [21] Y. Zhou, E.-Y. Ding, W.-D. Li, *Mater. Lett.* **2007**, 61, 5050.
- [22] J. Xue, F. Song, X. Dong, X.-W. Yin, Y. Liu, J.-M. Wu, C. Wang, X.-L. Wang, Y.-Z. Wang, *ACS Sustainable Chem. Eng.* **2018**, 7, 1973.
- [23] Y. Li, J. Zhang, C. Zhan, F. Kong, W. Li, C. Yang, B. S. Hsiao, *Carbohydr. Polym.* **2020**, 233, 115838.
- [24] G. D. Gesesse, C. Li, E. Paineau, Y. Habibi, H. Remita, C. Colbeau-Justin, M. N. Ghazzal, *Chem. Mater.* **2019**, 31, 4851.
- [25] C. M. Walters, K. R. Adair, W. Y. Hamad, M. J. MacLachlan, *Eur. J. Inorg. Chem.* **2020**, 2020, 3937.
- [26] T.-D. Nguyen, E. Lizundia, M. Niederberger, W. Y. Hamad, M. J. MacLachlan, *Chem. Mater.* **2019**, 31, 2174.
- [27] C. Wang, E. Paineau, H. Remita, M. N. Ghazzal, *Chem. Mater.* **2021**, 33, 6925.

- [28] C. Wang, J. Li, E. Paineau, H. Remita, M. N. Ghazzal, *Sol. RRL* **2023**, 2200929.
- [29] W. Hong, Z. Yuan, X. Chen, *Small* **2020**, 16, 1907626.
- [30] C. Yang, Y. Hirose, S. Nakao, T. Hasegawa, *Thin Solid Films* **2014**, 553, 17.
- [31] A. D. French, *Cellulose* **2013**, 21, 885.
- [32] C. Byrne, L. Moran, D. Hermosilla, N. Merayo, Á. Blanco, S. Rhatigan, S. Hinder, P. Ganguly, M. Nolan, S. C. Pillai, *Appl. Catal. B* **2019**, 246, 266.
- [33] P. A. DeSario, J. J. Pietron, T. H. Brintlinger, M. McEntee, J. F. Parker, O. Baturina, R. M. Stroud, D. R. Rolison, *Nanoscale* **2017**, 9, 11720.
- [34] K. Wang, Z. Bielan, M. Endo-Kimura, M. Janczarek, D. Zhang, D. Kowalski, A. Zielińska-Jurek, A. Markowska-Szczupak, B. Ohtani, E. Kowalska, *J. Mater. Chem. A* **2021**, 9, 10135.
- [35] J. Navas, A. Sanchez-Coronilla, T. Aguilar, N. C. Hernandez, D. M. de los Santos, J. Sanchez-Marquez, D. Zorrilla, C. Fernandez-Lorenzo, R. Alcantara, J. Martin-Calleja, *Phys. Chem. Chem. Phys.* **2014**, 16, 3835.
- [36] C. Cheng, W.-H. Fang, R. Long, O. V. Prezhdo, *JACS Au* **2021**, 1, 550.
- [37] T. Aguilar, J. Navas, R. Alcántara, C. Fernández-Lorenzo, J. J. Gallardo, G. Blanco, J. Martín-Calleja, *Chem. Phys. Lett.* **2013**, 571, 49.
- [38] D. W. Berreman, *J. Opt. Soc. Am.* **1972**, 62, 502.
- [39] D. Y. K. Ko, J. Sambles, *J. Opt. Soc. Am. A* **1988**, 5, 1863.
- [40] H.-G. Yoon, H. Gleeson, *J. Phys. D: Appl. Phys.* **2007**, 40, 3579.
- [41] R. C. Jones, *J. Opt. Soc. Am.* **1942**, 32, 486.
- [42] H. G. Yoon, H. F. Gleeson, *J. Phys. D: Appl. Phys.* **2007**, 40, 3579.
- [43] A. G. Dumanli, H. M. van der Kooij, G. Kamita, E. Reisner, J. J. Baumberg, U. Steiner, S. Vignolini, *ACS Appl. Mater. Interfaces* **2014**, 6, 12302.
- [44] D. Hewson, P. Vukusic, S. J. Eichhorn, *AIP Adv.* **2017**, 7, 065308.
- [45] R. Vidhya, M. Sankareswari, K. Neyvasagam, *Int. J. Tech. Res. Appl.* **2016**, 37, 42.
- [46] O. Deparis, S. R. Mouchet, B. L. Su, *Phys. Chem. Chem. Phys.* **2015**, 17, 30525.
- [47] J. Liu, H. Zhao, M. Wu, B. Van der Schueren, Y. Li, O. Deparis, J. Ye, G. A. Ozin, T. Hasan, B. L. Su, *Adv. Mater.* **2017**, 29, 1605349.
- [48] T. L. Madanu, S. R. Mouchet, O. Deparis, J. Liu, Y. Li, B. L. Su, *J. Colloid Interface Sci.* **2023**, 634, 290.
- [49] T. L. Madanu, L. Chaabane, S. R. Mouchet, O. Deparis, B. L. Su, *J. Colloid Interface Sci.* **2023**, 647, 233.
- [50] G. Colón, M. Maicu, M. C. Hidalgo, J. A. Navío, *Appl. Catal. B* **2006**, 67, 41.
- [51] W. Chen, Y. Wang, S. Liu, L. Gao, L. Mao, Z. Fan, W. Shangguan, Z. Jiang, *Appl. Surf. Sci.* **2018**, 445, 527.
- [52] M.-C. Wu, P.-Y. Wu, T.-H. Lin, T.-F. Lin, *Appl. Surf. Sci.* **2018**, 430, 390.
- [53] B.-A. Mei, J. Lau, T. Lin, S. H. Tolbert, B. S. Dunn, L. Pilon, *J. Phys. Chem. C* **2018**, 122, 24499.
- [54] M. Z. Hussain, B. van der Linden, Z. Yang, Q. Jia, H. Chang, R. A. Fischer, F. Kapteijn, Y. Zhu, Y. Xia, *J. Mater. Chem. A* **2021**, 9, 4103.
- [55] B. H. Lee, S. Park, M. Kim, A. K. Sinha, S. C. Lee, E. Jung, W. J. Chang, K. S. Lee, J. H. Kim, S. P. Cho, H. Kim, K. T. Nam, T. Hyeon, *Nat. Mater.* **2019**, 18, 620.
- [56] D. Zhong, Z. J. Zhao, Q. Zhao, D. Cheng, B. Liu, G. Zhang, W. Deng, H. Dong, L. Zhang, J. Li, J. Li, J. Gong, *Angew. Chem., Int. Ed.* **2021**, 60, 4879.
- [57] J. Zhao, M. Zhang, S. Wan, Z. Yang, C. S. Hwang, *ACS Appl. Mater. Interfaces* **2018**, 10, 1828.
- [58] V. Polliotto, S. Livraghi, A. Krukowska, M. V. Dozzi, A. Zaleska-Medynska, E. Selli, E. Giamello, *ACS Appl. Mater. Interfaces* **2018**, 10, 27745.
- [59] P. Basnet, E. Anderson, Y. Zhao, *ACS Appl. Nano Mater.* **2019**, 2, 2446.
- [60] M. A. Hossain, R. Al-Gaashani, H. Hamoudi, Al M. J. Marri, I. A. Hussein, A. Belaidi, B. A. Merzougui, F. H. Alharbi, N. Tabet, *Mater. Sci. Semicond. Process.* **2017**, 63, 203.